High-throughput all-optical postsynaptic plasticity map navigates connectome-guided Voltage-Seq

Veronika Csillag[1], Marianne Hiriart Bizzozzero[1], Joyce Noble[2], Björn Reinius[2], János Fuzik[1]*

[1] Department of Neuroscience, Karolinska Institutet, Stockholm, Sweden
[2] Department of Medical Biochemistry and Biophysics, Karolinska Institutet, Stockholm, Sweden

*Correspondence: janos.fuzik@ki.se

Abstract

Postsynaptic plasticity is not accessible as a selection criterion for molecular identification of neurons by single-cell RNA-sequencing (scRNA-seq). The currently available methods to find specific connection plasticity *ex vivo* have inherently low throughput. To overcome these limitations and pre-select neurons based on short-term postsynaptic plasticity for soma harvesting and subsequent scRNA-seq we created Voltage-Seq. First, we established all-optical voltage imaging and recorded the short-term postsynaptic plasticity of 6911 periaqueductal gray (PAG) neurons evoked by optogenetic activation of the ventromedial hypothalamic (VMH) input. Postsynaptic response-types were classified and spatially resolved in the entire innervated PAG. Next, to browse and identify all-optical responses, we built a quick on-site analysis named VoltView which incorporated the *a priori* VMH-PAG connectome database as a classifier. VoltView targetedly identifies postsynaptic neurons for somatic harvesting. We demonstrated the agility of Voltage-Seq in locating GABAergic PAG neurons, guided by an all-optical connectivity map and on-site classification in VoltView.

Main

Neuronal characterization and circuit connectivity testing is currently limited by the inverse relation of throughput and signal resolution. Labeling with anatomical or genetical tools is required to enrich neurons both for *ex vivo* electrophysiological recordings and for scRNA-seq. Patch-Seq[1-3] bridged these fields and pioneered to enrich neuronal subtypes for scRNA-seq based on intrinsic excitability, but still identified neurons to record based on anatomic or genetic labeling. Techniques are currently not available to label neurons based on their short-term postsynaptic plasticity, what in addition, can vary in an input-dependent manner. Furthermore, to date, subthreshold postsynaptic potentials (PSPs) of both polarities are measured by whole-cell patch-clamp which has inherently low throughput for population studies[4]. Enrichment of neurons for scRNA-seq based on short-term or long-term postsynaptic plasticity requires a high-throughput approach which can detect subthreshold and suprathreshold membrane potential changes. Genetically encoded fluorescent voltage indicators (GEVIs) [5, 6] provide a direct proxy to membrane voltage and can report changes of both polarities[5] with a temporal resolution that captures single action potentials (APs). Voltage imaging has high throughput[7] to potentially perform simultaneous connectivity testing on dozens of postsynaptic neurons. We set up all-optical voltage imaging implementing the recently introduced Voltron sensor[7] and we optimized Voltage-Seq, to all-optical voltage image short-term synaptic plasticity *ex vivo* and to select neurons for somatic harvesting and subsequent scRNA-seq. Furthermore, we complemented our approach with an interactive on-

site analysis named VoltView. First, we built a whole-structure synaptic connectome database of the VMH-PAG pathway. Next, we added a classifier to VoltView incorporating VMH-PAG postsynaptic classification as *a priori* knowledge. Voltage-Seq allows the on-site classification of specific postsynaptic response-types thus provides access to enrich sampling of neurons with specific synaptic connectivity and firing activity to enhance the molecular identification of protagonist circuit players of a synaptic connectome.

Results

All-optical postsynaptic voltage imaging

We established and optimized all-optical voltage imaging *ex vivo,* implementing the recently introduced Voltron[7] sensor, with fast kinetics. To interrogate the VHM-PAG postsynaptic connectome, we expressed Cre-recombinase and the Cre-dependent somatic targeting Voltron (Voltron-ST) co-injecting the two adeno-associated viruses (AAVs) in the PAG of wild type mice (Fig. 1a). With this viral combination we achieved a cell-type-independent Voltron-ST labeling in ~35-40% of PAG neurons (Extended Data Fig. 1a). We fluorescent-labeled the sensor with the Janelia Fluor®585 (JF-585) dye and configured the light path accordingly (Extended Data Fig. 1b). We optimized imaging acquisition speed to 600 Hz, where v-APs consisted of 3-4 points (Extended Data Fig. 1c), and a ~2-times increase in AP half-width was reported by a ~30% significant increase in v-AP half-width (Extended Data Fig. 1d,e). We simulated EPSPs (Extended Data Fig. 1f) in whole-cell voltage-clamp recordings paralleled by Voltron-imaging (Extended Data Fig. 1g,h) and validated that the sensor can even detect small ~2-3 mV excitatory (v-EPSPs) and inhibitory (v-IPSPs) PSPs. We validated that 585 nm illumination had a negligible cross-activation of Channelrhodopsin-2 (ChR2) (Extended Data Fig. 1i,m), with a maximal ~3 mV depolarization at the extreme 21 mW of 585 nm light tested (Extended Data Fig. 1k). Furthermore, we validated that optogenetically evoked synaptic release probability was not altered by any cross-activation (Extended Data Fig. 1l). For VMH-PAG all-optical imaging we also expressed ChR2 in the VMH (Fig 1a). We successfully all-optical-imaged both v-EPSPs and v-IPSPs and confirmed the signals with e-IPSPs recorded in an imaged cell (Fig. 1b). All-optical recordings revealed the 473 nm light-induced narrow “blue spike” artefacts. These served as time stamps of optogenetic stimulation (OS), had reversed polarity to v-APs, and were removed during analysis (Extended Data Fig. 1n). We encountered excitatory e-EPSP/ v-EPSP responses with a narrow concave profile (Fig. 1c) which widened upon hyperpolarization, while depolarization reversed them to a convex e-IPSP and v-IPSP. This showcased the fine detection of converging excitatory and inhibitory inputs with opposing polarities (Fig. 1c). We combined all-optical imaging and antagonist pharmacology to dissect a concave v-EPSP. Bath-application of 1 µM tetrodotoxin (TTX), with 5 mM 4-aminopiridin (4-AP) blocked AP firing, turned the concave v-EPSP profile into convex v-EPSP. Subtracting the two profiles resulted in a response with inhibitory polarity, which indicated that we all-optical imaged disynaptic inhibition (Fig. 1d). Imaging a rebound-bursting neuron confirmed the co-detection of multiple neuronal voltage events from large slow hyperpolarization, rhythmic depolarization to fast spiking (Fig. 1e). The involvement of GABA was predicted by the concave v-EPSPs during OS (Fig. 1e). Bath-application of γ-aminobutyric acid ionotropic receptor ($GABA_AR$) antagonist, Gabazine (10 µM) turned the rebound-bursting into onset-bursting. Remarkably, we all-optical imaged a circuit phenomenon which had not yet been described before. We observed PAG neurons alternating between excitatory and inhibitory responses across consecutive sweeps. We named this “Switch” response, where converging excitatory and inhibitory inputs prevailed in an alternate manner (Fig. 1f). Bath-

application of Gabazine (10 µM) eliminated the inhibitory input, further confirmed by the firing frequency increase during the sweeps (Fig. 1g). All-optical postsynaptic physiology has high sensitivity to detect the firing activity and separate or overlapping inhibitory and excitatory subthreshold responses. All-optical postsynaptic imaging can observe undisturbed circuit states without the perturbance of the membrane potential and the ionic milieu of the imaged neurons.

Classification of postsynaptic all-optical response types

We expressed eYFP with an AAV in VMH and prepared a 3D VMH-PAG axon density map (Extended Data Fig. 2a,b) to designate the optimal area to all-optical image the VMH-PAG connectome (Fig. 2a,b). To build a connectome database we all-optical voltage imaged 2 to 3 planes in each FOV, tile-covered the VMH-innervated PAG area with 6-7 FOVs on 5-7 brain slices per mouse in 7 mice and imaged 6911 neurons (Fig. 2b, Extended Data Fig. 2c). We detected the 30 to 70 somatic region of interests (ROIs) in each video implementing Cellpose segmentation[8] and extracted voltage-physiology (v-phys) traces (Fig. 2c). We detected basic features of AP peaks, subthreshold dynamics, v-EPSPs, v-IPSPs and burst activity from all 7 v-phys sweeps of each ROI v-phys trace (Fig. 2d). Periods of burst activity were detected based on subthreshold kinetics and validated by the corresponding firing frequency (Extended Data Fig. 2d). To confirm the origin of the ROI signals, we constructed the “Concentric” analysis, which validates somatic origin of v-phys traces using the detected basic features (i.e. AP number, AP amplitude and burst length) (Extended Data Fig. 2f,g). We generated an all-optical VMH-PAG postsynaptic connectome database with 87.4% of imaged postsynaptic PAG neurons connected to the VMH input (Fig. 2e) and OS of VMH terminals resulted in AP firing in 62.1% of the innervated neurons (Fig. 2e). We extracted 29 parameters of the all-optical postsynaptic responses (Extended Data Fig. 2f) and performed unbiased hierarchical clustering on the 6911 neurons to classify their VMH-PAG postsynaptic v-phys into 18 distinct clusters (Fig. 2f,g, Extended Data Fig. 2h). Within the VMH-PAG postsynaptic connectome we identified: persistent activity after the OS (cluster 1,4); rhythmic bursting with 3-4 Hz (cluster 8), burst upon each OS (cluster 5); time-locked single AP upon each OS (cluster 7); strongly depressing (cluster 10,6) and strongly facilitating short-term synaptic plasticity (cluster 9); facilitating paired-pulse (PP) plasticity (cluster 2,4,9,16); depressing PP plasticity (cluster 15); spontaneous firing activity preceding the OS (cluster 3,11,12,13,14); inhibitory responses (cluster 14); inhibitory responses with rebound firing or bursting (cluster 3); subthreshold response (cluster 17); weak or not detectable connection (cluster 18) (Fig. 2h). V-phys parameters well-mapped across v-phys types where suprathreshold activity dominated the all-optical responses of the cluster, referred to as “high synaptic drive” (Fig. 2i). For example, spike bimodality was highest in cluster 8, 5; the dynamics in burst length during the OS was increasing in cluster 9 and strongly decreasing in cluster 6; burst length could only be measured after the OS (Post-2) in cluster 1,3,4,11 (Fig. 2i). In summary, we built a VMH-PAG all-optical connectome database with well-defined clusters.

Spatial topography of postsynaptic connectome

We post-hoc extracted the XYZ coordinates of each 6911 imaged neuron and created the spatial map of our connectome (Extended Data Fig. 3a,b). On our VMH-PAG spatial axonal map we found high accordance of axonal density and maximal and minimal v-phys response intensity (Extended Data Fig. 3c,d,e). For spatial response-type-independent overview, the

PAG was divided to voxels, and the percentage of postsynaptic neurons within them fulfilling a criterion was calculated (Fig. 3a). The voxel-criterion of >3 v-PSP responses to the 20 Hz OS visualized a homogenous distribution of high-percentage voxels confirming a complete spatial coverage of detected connections in our connectome (Fig. 3b). The voxel-criterion of >18 v-PSPs during the 20 Hz OS visualized connection strength, displayed spatial patterns of stronger and weaker VMH innervation (Fig. 3c), suggesting functional topography. Voxel-mapping paired-pulse facilitation, a qualitative short-term synaptic plasticity property[9], highlighted a PAG subregion with high density of facilitating connections (Fig. 3d). Our all-optical connectome described whole-structure VMH-PAG connectivity on the quantitative and qualitative levels. Remarkably, mapping the anatomical density-core of the VMH-PAG connectome by v-phys cluster identity revealed spatial patterns (Fig. 3e). To test the spatial proximity within v-phys clusters, the average minimal distance (AMD) between neurons of the same cluster was compared to the chance-level AMD calculated by repeated shuffles of cluster identity (Fig. 3f). The observed AMDs were shorter than the AMDs expected by chance for most clusters, thus v-phys clusters also formed spatial clusters. Next, the AMD of neurons of distinct v-phys clusters was probed across all 18 clusters (Fig. 3g, Extended Data Fig. 3f) and was found to be significantly smaller than expected by chance between spatially intermingled clusters, such as cluster 2 and 4, cluster 10 and 1, and cluster 9 and 6 (Extended Data Fig. 3g). The AMD was found to be significantly larger than expected by chance between spatially segregated clusters with lower densities, such as cluster 9 and 13 or cluster 8 and 1 (Fig. 3g, Extended Data Fig. 3f,h). The side-by side visualization of v-phys cluster centroid distances and spatial cluster centroid distances suggested coherence of the two properties (Fig. 3h). The function of the two distances confirmed a pronounced correlation between v-phys cluster identity and spatial location (Fig. 3i). The high throughput of our whole-structure all-optical postsynaptic imaging had the resolution to reveal the organized topography of the VMH-PAG connectome from the v-phys data of 7 mice, which was to-date not accessible by any other approach.

On-site analysis of all-optical voltage imaging with VoltView

To make all-optical experimenting interactive, we developed VoltView. The “On-site” configuration of the package provides quick access to the basic features analyzed (AP peaks, Subthreshold kinetics, Burst activity) of 30-70 neurons in ~1 min (Fig. 4a). The “Offline” configuration runs deeper analysis to validate signal source with “Concentric” (Extended Data Fig. 2e), extracts APs with AP half-width and detects v-EPSPs and v-IPSPs in ~5 min (Fig. 4a). As proof of principle, we demonstrated how we located and validated burst firing of a neuron with VoltView. After acquisition and on-site analysis, VoltView opens an “ROI Explorer” for browsing postsynaptic responses where we chose an onset-bursting neuron with a detected burst on each sweep (Fig. 4,b). Guided by the position indication of the currently inspected ROI we recorded the neuron in whole-cell patch-clamp and deployed the same 20 Hz OS (Fig. 4,c2). Similarly, higher initial firing frequency with pronounced adaptation was observed. Next, we characterized the intrinsic excitability of the same neuron in the classical way with current injections in current-clamp mode (Fig. 4,c3) and confirmed the intrinsic burst firing which had been all-optical-imaged (Fig. 4c,4). The all-optical imaging companion VoltView thus could on-site reveal the identity of a neuron upfront and spatially guide the experimenter for further patch-clamp investigation. On-site analysis can provide comparison of analyzed features across different all-optical recordings of the same neurons. We attempted to identify postsynaptic responses with increased or decreased long-term burst plasticity evoked by a 50 Hz optogenetic high-frequency stimulation protocol (oHFS) (Fig. 4d). After

motion-correction of the repeatedly imaged FOVs, parameters of the same neurons were extracted and on-site-compared across imaging sessions (Rec1, Rec2) (Fig. 4d). On-site analysis had a 25%-change cutoff to identify ROIs with increased or decreased total burst length (Fig. 4d). VoltView successfully identified a neuron with robustly decreased bursting (Fig. 4e,g) where the rhythmic slow bursting turned into continuous firing after oHFS (Fig. 4e). A neighboring neuron displayed opposite change with increased burst length where interestingly the rhythmicity of bursts blended into an irregular tone across sweeps, well-shown by the sweep average (Fig. 4f,g). Importantly, the responses of both neurons in both Rec1 and Rec2 were highly stable across 7 sweeps taken during a 70 s time window, indicating that all-optical observation of neurons can capture a postsynaptic response rendered to a circuit state. Our VoltView analysis made *ex vivo* experimenting interactive with all-optical imaging and on-site selection of neurons based on user-defined firing property or connection plasticity features.

Connectome-guided Voltage-Seq

The extreme high throughput and high resolution of all-optical imaging moved *ex vivo* synaptic connectivity testing to the big data regime. We generated a VMH-PAG connectome database and combined it with VoltView to allow the on-site classification of specific postsynaptic response-types belonging to identified v-phys clusters. Suggested neurons were then harvested for subsequent scRNA-seq. We named the overall workflow Voltage-Seq. To test the ability of Voltage-Seq to locate neurons within the VMH-PAG connectome, we attempted to find GABAergic neurons which are sparsely distributed. GABAergic neurons of the PAG had been reported to be more depolarized and often spontaneously active to provide tonic inhibition[10]. We therefore selected cluster 3,12 and 13 from our all-optical connectome which had more than 50% of the neurons spontaneously firing (Fig. 2h). In our wild type VMH-PAG connectome database, spontaneous firing was exerted by a sparse population (8.2%) (Fig. 5a). Our spatial core-distribution of these three clusters revealed their overlap in the posterior part of PAG (Fig. 5b). Remarkably, in the coronal view, the neurons of the three clusters were restricted to dorsal (dPAG) and dorsolateral (dlPAG) parts of PAG, avoiding its lateral (lPAG) portions (Fig. 5b), which typically describes the distribution of GABAergic neurons in the PAG (Extended Data Fig. 4a). To validate the correlation of GABAergic identity and spontaneous firing, we all-optical voltage imaged 1436 GABAergic neurons in the posterior portion of the PAG of 4 VGAT-cre mice (Fig. 5c). The overall connection ratio was much lower (45.6%) than that in the wild type mice, which indicated a quantitative difference of the VMH-PAG inhibitory connectome *per se*. The ratio of spontaneously firing postsynaptic neurons was ~8-times higher (63.7%) in the GABAergic connectome (Fig. 5c), which indicated a potential correlation of the spontaneous firing activity and GABAergic nature. Based on this data we chose to test whether VoltView can assist with on-site v-phys classification to enrich the harvesting of sparse GABAergic neurons for Voltage-Seq. We expressed the Voltron-ST in the posterior portion of the PAG of wild type mice and expressed ChR2 in the VMH (Fig. 5d). During the on-site analysis VoltView used its classifier to suggest neurons belonging to cluster 3, 12 and 13 for somatic harvesting (Fig. 5e). We concentrated a sample of spontaneously firing PAG neurons by harvesting 60 neurons from 3 mice. As whole-cell recording is optional with all-optical imaging, the throughput of Voltage-Seq increased two-fold compared to Patch-seq (18-22 neurons/animal compared to 8-12 neurons/animal). Notably, the harvesting protocol was optimized for Voltage-Seq and tested with Smart-Seq2[11] and Smart-Seq3[12] (Fig. 5e, Extended Data Fig. 4b, see Methods). We checked for the detection of glial markers and found low level and sparse detection indicating that the clearance of harvesting was satisfactory (Extended

Data Fig. 4c). The GABAergic population ratio, based on in situ labeling with *Slc32a1* (vesicular GABA transporter) or *Gad1* (Glutamic acid decarboxylase) and *Slc17a6* (vesicular glutamate transporter) in the dPAG and dlPAG, was estimated to be ~15% (Fig. 5f). RNA-transcriptome revealed the neurotransmitter modality of the Voltage-seq-collected neurons with a remarkably high 64% (35/54) proportion of GABAergic neurons (Fig. 5f), confirming that we succeeded to enrich the sampling of GABAergic neurons of the VMH-PAG connectome.
Voltage-Seq could provide on-site access to neurons with specific synaptic connectivity and firing activity to enrich our molecular identity profiling of a sparse neuronal population, which we could not have found by chance in these proportions of the PAG.

Discussion

By optimizing a multi-layered approach, we created the Voltage-Seq workflow which combines anatomical, physiological, and molecular approaches on-site, to robustly increase the efficacy of postsynaptic circuit measurements and molecular classification of neurons. All-optical postsynaptic physiology with our interactive VoltView package has two mutually reinforcing modes of operation. One being the high-throughput quick accumulation of fine-detailed postsynaptic observations to generate a connectome database and the other being the on-site identification using the previously generated database. Voltage-Seq could potentially identify postsynaptic response- or neuronal types across multiple connectome databases. All the regions of the mammalian brain receive synaptic inputs from a multitude of sources. Genetical or anatomical targeting of a chosen postsynaptic population could allow the generation and comparison of converging connectome datasets to explore the input-specific synaptic control of the chosen population. Moreover, high-throughput connectome-based analysis in mouse models of mental illnesses could provide an overview of the short-term and long-term synaptic plasticity landscape of one or multiple brain areas of the same mouse. Such a comprehensive map could highlight the focal points of circuit imbalance to narrow down the sampling of Voltage-Seq-harvested neurons and detect gene expression changes or reveal the identity of postsynaptic neuronal types in circuit motifs of imbalanced circuits. All-optical voltage imaging for Voltage-Seq could set new standards of circuit plasticity recordings and subsequent investigations for its flexibility and high experimental potential and would be more accessible to a wider range of neuroscience fields as it needs less equipment and hands-on skills of the experimenter compared to the fine skills of patch-clamp-electrophysiologists which require years of dedicated practice to develop.

Methods & Protocols

Animals

Experiments were conducted using adult male and female mice, wild type C57BL/6J (Charles River Laboratories) or the transgenic mouse line VGAT-Cre: *B6J.129S6(FVB)-Slc32a1*$^{tm2(cre)Lowl}$*/MwarJ*, Jackson stock no. 028862. All transgenic mice used in experiments were heterozygous for the transgenes. Mice were group housed, up to five per cage, in a temperature (23°C) and humidity (55%) controlled environment in standard cages on a 12:12hr light/dark cycle with *ad libitum* access to food and water. All procedures were approved and performed in accordance and compliance with the guidelines of the Stockholm Municipal Committee (approval no. N166/15 and 7362-2019).

Animal cohorts

Anatomy and histology: n = 2 pAAV-CAG-GFP
Patch-clamp electrophysiology: n = 7 pAAV-hSyn-hChR2(H134R)-EYFP
Voltage-imaging and optimalization: n = 21 pENN.AAV.hSyn.Cre.WPRE.hGH; pAAV-hsyn-flex-Voltron-ST; pAAV-hSyn-hChR2(H134R)-EYFP

Viral constructs

All purified and concentrated adeno-associated viruses (AAV) were purchased from Addgene.

Anatomy and histology

pAAV-CAG-GFP (AAV5); Addgene, cat. no. 37825-AAV5; (at titer ≥ 7×10e12 viral genomes/ml)

Voltage-imaging

pAAV-hsyn-flex-Voltron-ST (AAV1); Addgene, cat. no. 119036-AAV1; (at titer ≥ 2×10e12 viral genomes/ml)
pAAV-hSyn-hChR2(H134R)-EYFP (AAV5); Addgene, cat. no. 26973-AAV5; (at titer ≥ 7×10e12 viral genomes/ml)
pENN.AAV.hSyn.Cre.WPRE.hGH (AAV1); Addgene, cat. no. 05553-AAV1; (at titer ≥ 1×10e13 viral genomes/ml)

Viral injections

General procedure

Mice were anesthetized with isoflurane (2%) and placed into a stereotaxic frame (Harvard Apparatus, Holliston, MA). Before the first incision the analgesic Buprenorphine (0.1 mg/kg) and local analgesic Xylocain/Lidocain (4 mg/kg) was administered subcutaneously. Body temperature of the mice was maintained at 36 °C with a feedback-controlled heating pad. For viral injections a micropipette attached on a Quintessential Stereotaxic Injector (Stoelting, Wood Dale, IL) was used. Injections were done with the speed of 50 nl/minute. The injection pipette was held in place for 5 min after the injection before being slowly (100 µm/s) retracted from the brain. The analgesics Carprofen (5 mg/kg) was given at the end of the surgery, followed by a second dose 18-24h after the surgery.

Labeling strategies

For anatomical characterization and electrophysiological recordings of the VMH-PAG pathway in C57BL/6J mice, 0.3µl pAAV-CAG-GFP or pAAV-hSyn-hChR2(H134R)-EYFP was unilaterally injected into the VMH (coordinates: AP -1.45 mm, ML 0.25 mm, DV -5.25 mm). Targeting of the PAG was achieved by 1 (coordinates: AP -4.1 mm, ML 0.2 mm, V -1.6 mm) or 2 (coordinates: AP -3.9 mm and AP -4.3 mm, ML 0.2 mm, V -1.6 mm) unilateral injections of 0.3µl of 1:1 mixture of pENN.AAV.hSyn.Cre.WPRE.hGH and pAAV-hsyn-flex-Voltron-ST.

Histology

General procedure

Mice were deeply anaesthetized with Na-pentobarbital (60mg/kg) and transcardially perfused with 0.1M PBS followed by 4% paraformaldehyde in PBS 0.1M. Brains were removed and post-fixed in 4% paraformaldehyde in PBS 0.1M overnight at 4°C and then washed and stored in 0.1M PBS. Coronal, 50 µm slices were cut using a vibratome (Leica VT1000, Leica Microsystems, Nussloch GmbH, Germany). The sections were washed in 0.1M PB and mounted on glass slides (Superfrost Plus, Thermo Scientific) and coverslipped (Thermo Scientific) using glycerol: 1x PBS (50:50).

Histology of biocytin filled neurons

250 µm thick brain slices containing biocytin-filled neurons and voltron-JF585 labeling were post-fixed in 4% paraformaldehyde in phosphate-buffer (PB, 0.1M, pH 7.8) at 4 °C overnight. Slices were repeatedly washed in PB and cleared using CUBIC protocol[13]. First “CUBIC reagent 1” was used (25 wt% urea, 25 wt% N,N,N’,N’-tetrakis(2- 764 hydroxypropyl) ethylenediamine and 15 wt% polyethylene glycol mono-p-isooctylphenyl 765 ether/Triton X-100) for 1 day at 4 °C. After repeated washes in PB, biocytin localization was visualized using Alexa Fluor 633-conjugated streptavidin (1:1000, RT 3 hours). For NeuN staining primary antibody (Millipore, MAB377,1:1000) was incubated overnight at 4 °C and after repeated washing with PB, 2nd antibody (Jackson, Cy5, Code:715-175-151) was incubated for 3h RT. Slices were then re-washed in PB and submerged in “CUBIC reagent 2” (50 wt% sucrose, 25 wt% urea, 10 wt% 2,20,20’- 768 nitrilotriethanol and 0.1% v/v% Triton X-100) for further clearing. Slices were mounted on Superfrost glass (Thermo Scientific) using CUBIC2 solution and covered with 1.5 mm cover glasses.

Confocal imaging

All confocal images were taken using a Zeiss 880 confocal microscope. CUBIC cleared sections after slice electrophysiology and biocytin or NeuN staining were acquired as z-stacks using a Plan-Apochromat 20x/0.8 M27 objective (imaging settings: frame size 1024x1024, pinhole 1AU, Bit depth 16 bit, speed 6, averaging 4). For viral expression overview of coronal cut VMH or PAG sections were acquired with a Plan-Apochromat 20x/0.8 M27 objective (imaging settings: frame size 1024x1024, pinhole 1AU, Bit depth 16 bit, speed 7, averaging 2). Processing of images was either done in ImageJ (NIH, USA) or Imaris 7.4.2 (Oxford Instruments, UK).

Brain slice preparation

First, mice were anesthetized with intraperitoneal injection of 50 µl Na-pentobarbital (60 mg/kg) and transcardially perfused with 4-8 °C cutting solution, containing (in mM): 40 NaCl, 2.5 KCl, 1.25 NaH2PO4, 26 NaHCO3, 20 glucose, 37.5 sucrose, 20 HEPES, 46.5 NMDG,

46.5 HCl, 1 L-ascorbic acid, 0.5 CaCl2, 5 MgCl2. Next, brain was carefully removed and 250 µm thick coronal slices were cut with a vibratome (VT1200S, Leica, Germany) in the same 4-8 °C cutting solution. Next, slices were incubated in cutting solution at 34°C for 13 minutes, and kept until recording at room temperature in artificial cerebrospinal fluid (aCSF) solution containing (in mM): 124 NaCl, 2.5 KCl, 1.25 NaH2PO4, 26 NaHCO3, 20 glucose, 2 CaCl2, 1 MgCl2. For Voltron-imaging, slices were incubated at room temperature in Janelia-Fluor 585 HaloTag (JF-dyes, Janelia) ligands. JF-dyes were dissolved in DMSO to a stock of 1 µM and further diluted to 50 nM in aCSF before use. All solutions were oxigenated with carbogen (95% O2, 5% CO2). All constituents were from Sigma-Aldrich.

Electrophysiology

C57BL/6J mice were injected with pAAV-hSyn-hChR2(H134R)-EYFP at 10-11 weeks and recorded 12-13 weeks of age (for details on the virus injection see “Viral injections” above. For patch-clamp recordings, brain slices were superfused with 33-34°C aCSF at a rate of 4-6 ml/min. Neurons were visualized using a 60x water-immersed objective (Olympus, Tokyo, Japan) in a DIC differential interference contrast (DIC) microscopy on an Olympus BX51WI microscope (Olympus, Tokyo, Japan). Patch borosilicate (Hilgenberg, Germany) pipettes, 7-10 MΩ pulled using a horizontal puller (P-87 Sutter Instruments, Novato, CA, USA) were filled with K-gluconate-internal solution containing (in mM): 130mM K-gluconate, 5mM KCl, 10mM HEPES, 10mM Na2-phosphocreatine, 4mM ATP-Mg, 0.3mM GTP-Na, 8 biocytin, 0.5 ethyleneglycol-bis(2-aminoethylether)-*N*,*N*,*N′*,*N′*-tetraacetate (EGTA), (pH 7.2 set with KOH). Signals were recorded with an Axon MultiClamp 700B amplifier and digitized at 20 kHz with an Axon Digidata 1550B digitizer (Molecular Devices, San Jose, CA, USA). Neurons recorded in current-clamp mode were held at a membrane potential of -60 mV. “AP threshold” (mV) was defined as the voltage point where the upstroke’s slope trajectory first reached 10 mV/ms. “AP half-width” (ms) was measured at half the maximal amplitude of the AP. All parameters were measured by procedures custom-written in MATLAB (MathWorks, USA). For measuring firing pattern 1 second long positive current injection was applied to the neuron. Pipette capacitance was compensated, liquid junction potential was not corrected. The synaptic properties of VMH projection onto PAG neurons were probed using multiple light pulse train protocols with 2 ms blue light pulses with ~2.5 mW light power from a SpectraX (Lumencor, USA) LED light source. In some experiments we bath applied TTX (1µM; Tocris) and 4-AP (5 mM; Sigma-Aldrich) to isolate monosynaptic responses. Inhibitory currents in some cases got pharmacologically blocked by bath application $GABA_A$ antagonist Gabazine (10µM; Sigma-Aldrich).

Voltage imaging

After 4-5 weeks of Voltron-ST expression, mice were sacrificed and ex vivo brain slices of 250 µm were prepared. After ~30 min of incubation in 50 nM Janelia-Fluor 585 dye dissolved in aCSF, slices were transferred to the recording chamber of the electrophysiology setup. For the imaging we used a digital sCMOS camera (Hamamatsu Orca Fusion-BT), frame triggers were sent to the camera with a Arduino Micro microcontroller (Arduino Uno) with 600 Hz. For all-optical imaging we used a dual-band excitation filter (ZET488/594, Chroma) to excite the JF-585 and deliver 473 nm light for optogenetic stimulation. The 585 nm light excitation intensity was ~10 mW/mm2 at the slice plane and was delivered by Spectra X (Lumencore) LED light source. JF-585 fluorescent emission was collected with a 20X 1.0 NA water immersion objective (XLUMPLFLN20XW Plan Fluorit, Olympus). Emitted light was separated from the excitation light with a band-pass emmission filter (ET645/75, Chroma) and with a

dichroic mirror (T612lprx, Chroma). Magnification was decreased with U-ECA magnification changer to 0.5x. To acquire videos we used the free LiveImage software triggered by the Arduino to synchronize acquisition with the frame triggers.

Voltage-Seq

VoltView analysis

The on-site and offline analyis was written in MATLAB (MathWorks) using custom-written scripts which are going to be available on github upon acceptance. In major steps, the recorded videos are imported and ROIs are segmented from contrast-tuned frame averages which had been optimized from Voltron-JF585 imaging. For segmentation we used Cellpose. After the detection of ROI contours we designated concentrical ROIs (Inner and Outer) around the somatic ROI and extracted the signal traces. Basic features, AP peaks, subthreshold trace, Buirst detection were done in custom-written scripts. Using the 3 ROIs we compared the amplitude of APs and the length of bursts across the somatic, inner and outer ROI and discarded neurons where the signal amplitude or burst intensity did not decrease or increased from the somatic ROI towards the inner and outer ROIs. Traces were denoised and all the calculated values and features were stored in struct variables so that VoltView can use them fro the ROI explorer plotting and for the on-site analysis.

Neuronal soma harvesting

After voltage-imaging of each FOV and consequennt VoltView on-ste analysis, we approached the selected somas one-by-one with a harvesting pipette (1.8-2.5 MΩ) containing (in mM): 90 KCl, 20 MgCl2. The entire soma of the selected neuron was aspirated into the pipette within a few seconds by applying mild negative pressure (-50 mPa) measured with a manometer. Switching from DIC to the fluorescent optics to visualize the Voltron-expressing neurons during and after aspiration could confirm the succesful harvesting process. Next, the harvesting pipette was pulled out of the recording chamber and then with the micromanipulator, carefully navigated over and inside a 0.2 ml tube under visual guidance observed by a 4X Olympus air objective (Olympus, Tokyo, Japan). Applying positive pressure, the harvested neuron (~0.5 µl) was ejected into a 2 µl drop of lysis buffer consisting of 0.15% Triton X-100, 1 U/µl TaKaRa RNase inhibitor, 2.5 mM dNTP, 17.5 mM DTT and oligo dT primer (2.5 µM) pre-placed in the very tip of the 0.2 ml tight-lock tube (TubeOne). Through the 4X air objective we could observe the line of small air bubbles coming out of the harvesting pipette tip into the lysis buffer as a confirmation of the completed ejection. The resultant sample (~2,5 µl) was spun down (5 s), placed to dry ice and stored at -80 °C, later subjected to in-tube reverse transcription (RT).

Single-cell RNA sequencing

Library prep:

SS2 and SS3 libaries were prepared as previously described except for the following changed: SS2 cDNA was amplified for 22 cycles and SS3 cDNA was amplified for 24 cycles. SS2 and SS3 cDNA (1ng and 100pg, respectively) were tagmented and amplified with custom 10bp indexes. Libraries were sequenced using a 150 cycle Nextseq 550 kit (paired end, 74bp reads).

Sequencing QC

Reads were aligned with the mm10 genome using zUMIs (version 2.9.5) using STAR (2.7.2a) with transcript annotations from GENCODE (version M25). Quality control reports for genes detected was performed with intron+exon alignments from zUMIs. Qualimaps was used to report the total reads aligned to intronic and exonic regions.

Differential expression and clustering

All expression analyses were performed with exonic reads only. The package Seurat in R was used to perform PCA and subsequent unbiased clustering.

Anatomical 3D mapping

Spatial mapping of imaged neurons was done using the common coordinate framework 4 (CCF4)[14]**.** X and Y coordinates were extracted form the videos relative to the top left corner and when Z coordinates were identified, the FOVs were mapped using „rails" generated with SHARP-track (Extended Data Fig 3a). The package is originally used to track electrodes, but it is higly suitable for constructing reference points or lines and extract the coordinates to support 3D mapping. Our reference lines went all along the A-P axis of PAG on the most dorsal, lateral and ventral edges and within the PAG they were spaced by the distance of the size of FOVs recorded.

Axonal mapping

Each coronal cut PAG brain section was manually mapped to an AP coordinate (z) and x-y coordinate for each fluorescent image pixel (axonal fluorescent labeling) was segmented out in ImageJ. For mapping coronal slices of axonal masks we used the reference lines generated with SHARP-track.

Data analysis

Classification and clustering of v-phys

Parameters for hierarchical clustering were extracted from the v-phys traces by custom-written routines in MATLAB (MathWorks). Agglomertive clustering was done by ward's algoritm, Euclidean distance for the cutoff and for definition of the number of clusters was chosen based on the slope-change of number of clusters vs the distance-cutoff.

Spatial cluster density

The observed minimal distances in space from a reference cell to a cell in the target cluster were calculated, as well as the expected minimal distances by chance, based on 1000 shuffles of cluster identity, for all cells. The distance metric was calculated for each cell by:

$$\frac{Observed - \frac{1}{n}\sum_{n=1}^{1000} expected(n)}{Observed + \frac{1}{n}\sum_{n=1}^{1000} expected(n)}$$

and is in range -1:1, where negative values indicated that the minimal distance of the reference cell to a cell in the target cluster is smaller than by chance and positive values indicated greater distance than by chance.

References

1. Fuzik, J. et al. Integration of electrophysiological recordings with single-cell RNA-seq data identifies neuronal subtypes. *Nat Biotechnol* **34**, 175-183 (2016).
2. Cadwell, C.R. et al. Electrophysiological, transcriptomic and morphologic profiling of single neurons using Patch-seq. *Nat Biotechnol* **34**, 199-203 (2016).
3. Marx, V. Patch-seq takes neuroscience to a multimodal place. *Nat Methods* **19**, 1340-1344 (2022).
4. Sakmann, B. & Neher, E. Patch clamp techniques for studying ionic channels in excitable membranes. *Annu Rev Physiol* **46**, 455-472 (1984).
5. Bando, Y., Sakamoto, M., Kim, S., Ayzenshtat, I. & Yuste, R. Comparative Evaluation of Genetically Encoded Voltage Indicators. *Cell Rep* **26**, 802-813.e804 (2019).
6. Kralj, J.M., Douglass, A.D., Hochbaum, D.R., Maclaurin, D. & Cohen, A.E. Optical recording of action potentials in mammalian neurons using a microbial rhodopsin. *Nat Methods* **9**, 90-95 (2011).
7. Abdelfattah, A.S. et al. Bright and photostable chemigenetic indicators for extended in vivo voltage imaging. *Science* **365**, 699-704 (2019).
8. Stringer, C., Wang, T., Michaelos, M. & Pachitariu, M. Cellpose: a generalist algorithm for cellular segmentation. *Nat Methods* **18**, 100-106 (2021).
9. Jackman, S.L. & Regehr, W.G. The Mechanisms and Functions of Synaptic Facilitation. *Neuron* **94**, 447-464 (2017).
10. Park, C. et al. T-type channels control the opioidergic descending analgesia at the low threshold-spiking GABAergic neurons in the periaqueductal gray. *Proc Natl Acad Sci U S A* **107**, 14857-14862 (2010).
11. Picelli, S. et al. Smart-seq2 for sensitive full-length transcriptome profiling in single cells. *Nat Methods* **10**, 1096-1098 (2013).
12. Hagemann-Jensen, M. et al. Single-cell RNA counting at allele and isoform resolution using Smart-seq3. *Nat Biotechnol* **38**, 708-714 (2020).
13. Susaki, E.A. et al. Whole-brain imaging with single-cell resolution using chemical cocktails and computational analysis. *Cell* **157**, 726-739 (2014).
14. Wang, Q. et al. The Allen Mouse Brain Common Coordinate Framework: A 3D Reference Atlas. *Cell* **181**, 936-953.e920 (2020).

Fig. 1: ***All-optical postsynaptic voltage imaging***

All Voltron traces were reversed. **a,** Scheme of viral expression of ChR2 in the VMH-PAG pathway and Voltron in the PAG. In the bottom ChR2 (green) and Voltron (gold) labeling in the PAG (scale bar, 10 µm) **b,** Scheme of simultaneous all-optical voltage imaging and whole-cell patch-clamp recording. Right, v-phys traces (average of 7 traces, gold) of three neurons (1,2,3) from top to bottom: neuron with no connection (1) neuron with excitation (v-EPSP) (2) and inhibition (v-IPSP) (3), and e-phys trace (average of 7 traces, black) of the whole-cell-recorded neuron (3) confirmed inhibitory postsynaptic responses (e-IPSP). **c,** Left, schematic illustration of a PAG neuron receiving both excitatory and inhibitory synaptic inputs during OS while voltage imaging. Side by side e-phys (average of 5 traces, black) and v-phys (average of 5 traces, gold) traces at different command voltages (-31 mV, -52 mV, -64 mV) with inhibitory input dominating (e-IPSP, v-IPSP) at most depolarized (-31 mV) and excitatory input dominating (e-EPSP, v-EPSP) at most hyperpolarized (-64 mV) command voltages. Bottom, voltage imaging could detect converging excitatory and inhibitory synaptic signal kinetics, which displayed a concave profile, while exclusively inhibitory (3) or only excitatory (2) synaptic responses had a convex profile. **d,** Left, all-optical v-phys (average of 7 traces, gold) in aCSF (A) and in TTX (1 µM)/4-AP (5 mM) (B) with the moving averages below (average of 7 traces, red). Right, subtraction of moving averages of A and B to extract the disynaptic inhibitory signal component (blue) (A-B) eliminated by TTX/4-AP. Bottom right, scheme of all-optical voltage imaging of a PAG neuron receiving excitation from VMH and disynaptic inhibition from local PAG circuitry. **e,** Top left, all-optical voltage imaging (3 consecutive traces, Inhibition, blue) of a PAG neuron showed inhibition during opto-stim of VMH input in aCSF and exerted rebound burst firing after the opto-stim (Rebound burst); same PAG neuron (3 consecutive traces, Excitation, red) in Gabazine (10 µM) showed elimination of the $GABA_A$-mediated inhibition resulting in onset burst firing during opto-stim (Onset burst). Right, enlarged all-optical v-EPSPs and v-IPSPs in a concave profiled signal (average of 7 traces, Inhibition, blue) and only v-EPSPs after Gabazine pharmacology (average of 7 traces, Excitation, red). Dashed gray line indicates baseline before opto-stim. **f,** Left, all-optical voltage imaging of a “switch” response in six consecutive traces, with excitatory (1,3,5, odd, red) and inhibitory (2,4,6, even, blue) responses, (divided to segments (1-5) for measuring v-APs frequency). Right, Gabazine (10 µM) block of $GABA_A$-mediated inhibition eliminated hyperpolarizing synaptic responses resulting in only increased firing activity during opto-stim (divided to segments (1-5) for measuring v-APs frequency). **g,** Top, insert of v-traces of “switch” response in aCSF with the first two opto-responses of excitatory (6 traces with average, red) and inhibitory (6 traces with average, blue), and plot of firing frequency across segments (1-5) in bottom, insert of v-traces of “switch” response in Gabazine (10 µM) with first two opto-responses of excitatory (6 odd traces with average, red) and inhibitory (6 even traces with average, blue). Regardless of baseline firing frequency, all traces had increased AP firing rates.

Fig. 2: Classification of all-optical postsynaptic response types

All Voltron traces were reversed. **a,** Scheme of viral GFP labeling of VMH-PAG (left) and coronal sections of our 3D axonal map shows PAG areas with high VMH axonal coverage (right). **b,** Example of a FOV with Voltron-expressing PAG neurons and the illustration of tile-covering PAG slices for all-optical imaging (left) 3D plot of PAG with all the 6911 neurons of our all-optical connectome (right). **c,** representative FOV of Voltron-expressing PAG neurons (top), a contrast-tuned version of the same frame average with the yellow contours of segmented ROIs (middle), example v-phys trace extracted from an ROI (bottom). **d,** Basic feature detection of action potentials (APs), subthreshold kinetics (Subthr), Burst activity, v-EPSPs and v-IPSPs. **e,** t-SNE plot of the VMH-PAG v-phys connectome color coded by the

average number of detected v-IPSPs (blue) or average number of v-EPSPs (shades of red for ranges: 1-5;5-10;11-15;16-20) (top), same plot color coded by the latency of the first AP detected during the OS (bottom). **f,** Polar dendrogram of agglomerative hierarchical clustering with the identified clusters numbered and colored. **g,** t-SNE plot of the identified v-phys clusters, numbering and color code is identical to f. **h,** Scheme on top details the temporal segments of all-optical sweeps with Op-1: first half of OS, Op-2: second half of OS, Post-1: first half of after-OS, Post-2: second half of after-OS. Representative all-optical v-phys traces illustrate postsynaptic v-phys responses of the identified v-phys clusters (color code and number is identical to f and g) blue bars indicate the 20 Hz 473 nm light stimulation. **i,** t-SNE of the VMH-PAG postsynaptic v-phys (gray), cropping the "High synaptic drive" clusters, which are enlarged in the following t-SNEs mapping clustering parameters. Abbreviation in brackets for each parameter indicates the temporal segments (in h) from where the parameters were extracted.

Fig. 3: Spatial topography of postsynaptic connectome

a, t-SNE of the VMH-PAG postsynaptic v-phys in gray indicating that no distinction was made between PAG neurons for the voxel-mapping of the connectome. 3D PAG model of hemisphere subdivided to voxels (grid) with one voxel in the middle (red). Illustration of a 200x200 µm voxel and the quantification of neurons inside the voxel fulfilling a criterion that defined the color code from 0% (blue) to 100% (red) and the transparency with 0% being invisible. **b,** 3D PAG model with voxel-mapping of overall VMH connectivity (top), example all-optical responses fulfilling the low-cut criterion of displaying >3 PSPs (bottom). **c,** 3D PAG model with voxel-mapping of strong VMH synaptic connectivity (top), example all-optical responses fulfilling the low-cut criterion of displaying >18 PSPs (bottom). **d,** 3D PAG model with voxel-mapping paired-pulse facilitation (PP) (top), example all-optical responses of postsynaptic neurons exerting facilitating PP, insert shows first two v-EPSPs with green line highlighting the facilitation (bottom). **e,** t-SNE of the VMH-PAG postsynaptic v-phys, color coded by cluster identity (Fig 2g,h). 3D PAG model of one hemisphere for each v-phys cluster with the density-core mapping of postsynaptic neurons of the cluster. Colors from red to blue go from highest to lowest spatial density, transparency follows the color code with blue being invisible. **f,** The observed average minimal distance (AMD) from a neuron to another neuron of the same cluster, versus the AMD expected by chance calculated by repeated shuffles of cluster identity, error bars: ±SEM (bootstrapped). **g,** AMD of neurons of distinct v-phys clusters was probed across all 18 clusters in 324 comparisons. * = p-value < 3*10^(-5). **h,** side-by side visualization of v-phys cluster centroid distances and spatial cluster centroid distances, all axes are cluster labels. **i,** plot of v-phys cluster centroid distances versus spatial cluster centroid distances, colors code cluster identity.

Fig. 4: *On-site analysis of all-optical voltage imaging with VoltView*

All Voltron traces were reversed. **a,** Illustration of the on-site analysis of v-phys. From left to right in chronological order. **b,** User interface of VoltView with the ROI explorer. The enlarged insert on the left demonstrates ROI spatial indication with the number of the corresponding all-optical recording. The enlarged insert on the right shows the recorded sweeps with the detected spikes and bursts. **c,** 1. FOV of Voltron-expressing PAG neurons (top), white arrow points at the neuron chosen for whole-cell patch clamp recording based on bursting detected (white) on its v-phys sweeps (scale is 20 µm). All-optical imaged v-phys sweeps of a neuron with onset-bursts on each sweep (green lines under the sweeps). 2. Scheme of the experiment (top), 3 e-phys traces (bottom), 20 Hz OS during whole-cell patch clamp recording confirmed the onset-bursting which was visible during v-phys recording in 1. 3. Schematic figure with the

same Voltron expressing neuron during whole-cell patch clamp recording (top). As a response to current injections, the neuron showed an intrinsic bursting firing pattern. 4. Confocal image of the biocytin filled neuron (top). Insert with VMH axons (green), Voltron (orange) and biocytin (blue) (below). **d,** Multiple video comparison is a feature of VoltView. Rec1 and Rec2 was recorded in the same FOV, before and after 50 Hz oHFS, VoltView extracts parameters of the same neurons and compare them before and after stimulation. Decreased bursting is indicated with blue ROI contours, increased bursting is indicated with red ROI contours. **e,** Cell1: neuron which initially responded with bursts to the 20 Hz OS and after high frequency (50 Hz) stimulation the response shifted towards continuous firing. Bottom sweep is the average of the 7 sweeps above. **f,** Cell2: initially exerted rhythmic bursts during OS and after the oHFS responded to the 20 Hz OS with prolonged bursts, losing rhythmicity. The last sweep is the average of the 7 sweeps above. **g,** Line plots show comparison of total burst lengths before (black) and after oHFS (Cell1 is blue, Cell2 is red). Dots represent the total burst lengths in every sweep.

Fig. 5: *Connectome-guided Voltage-Seq*

a, Pie chart of detected connections in our wild type all-optical VMH-PAG connectome, and pie chart of spontaneously firing postsynaptic neurons within the VMH-PAG connectome. **b,** 3D PAG model of one hemisphere for v-phys cluster 3,12,13 with the density-core mapping of postsynaptic neurons of the three clusters (left), coronal bins of PAG (2: 3,65-3,95; 3:3,95-4,25; 4: 4,25-4,55, 5: 4,55-4,85) merging the spatial coordinates of cluster 3,12,13. (right) **c,** Injection scheme of ChR2 and Voltron-ST expression in the posterior portion of PAG of VGAT-Cre mice (left), pie chart of detected connections in our VGAT-cre all-optical VMH-PAG connectome, and pie chart of spontaneously firing postsynaptic neurons within the inhibitory VMH-PAG connectome (right). **d,** Injection scheme of ChR2 and Voltron-ST expression in the posterior portion of PAG of wild type mice. **e,** Voltage-Seq workflow with: all-optical voltage imaging; on-site analysis with classification (classifier efficacy for each cluster on the bar plot color coded by cluster identity); VoltView suggests ROIs; soma harvesting (upper row) with expel (bottom row) under 4X magnification validated by air bubbles in the tube upon ejection of the lysis buffer (LB); cDNA library preparation and scRNA-seq. **f,** In situ hybridization (ISH) from the opensource Allen ISH database with inverted colors for VGAT (Slc32a1), GAD67 (Gad1) and VGLUT2 (Slc17a6) with pie chart of estimation of the relative proportion of GABAergic to Glutamatergic neurons (left), bar plot of Voltage-Seq RNA-transcriptome with the expression of *Voltron-ST, Slc32a1, Gad2, Gad1, Slc17a6, Got1, Gabra1, Grina, Gria2 Tuba1a*, with pie chart of the relative proportion of GABAergic to Glutamatergic neurons based on *Gad1, Gad2, Slc32a1* expression (right), minor ticks are 5 and 10 TPM from left to right.

Extended Data Fig.1: Optimization of all-optical voltage imaging

All Voltron traces were reversed except in panel **h. a,** NeuN staining and Voltron labeling with JF-585 (left, Scale bar is 20 µm). Scheme of Voltron-expressing AAV injection to PAG, hive plot (mean±sd) of the percentage of Voltron-expressing neurons/total number of neurons in randomly designated areas of PAG. **b,** Optical setup of all-optical voltage imaging *ex vivo*. **c,** Scheme of simultaneous cell-attached patch-clamp recording and voltage imaging (top left), APs from a PAG neuron with time-aligned traces of e-phys (black) and v-phys (gold) from the same neuron (top right). Insert of v-phys trace acquired at 600 Hz framerate with AP peaks (Peak points) and points between AP-threshold and peak (Spike points), dashed line marks AP-threshold (bottom). **d,** E-phys trace at 0 pA (light gray) and 50 pA (dark gray) depolarizing current injection with the corresponding v-phys traces at 0 pA (gold) and 50 pA (brown) (left).

AP shape of e-phys (light gray, dark gray) and v-phys spikes (gold, brown) at 0 pA and 50 pA current injection (right). **e,** Half-width of APs compared across 0 pA and 50 pA current injection of e-phys (p = 1,9e-49) and v-phys (p = 6,4e-16) recordings (***p<0.001). **f,** Symmetric voltage command to test the subthreshold sensitivity of the Voltron sensor. The applied voltage command had amplitudes of 8, 10, 5, 3 mV and -8, -10, -5, -3 mV. **g,** Voltron-expressing neurons during imaging and whole-cell patching in 20x magnification (top). Std of dF/F of the whole-cell-recorded neuron, with the surrounding neurons not depolarized (bottom). **h,** Scheme of simultaneously voltage-imaged and whole-cell recorded neuron (top). Soma of a Voltron-expressing neuron, representing the pixel-binning for the surface plots. Application of the symmetric voltage command in whole-cell voltage-clamp during voltage imaging, top is e-phys recording, below is the corresponding v-phys trace from the same recorded neuron (avg. of 10 sweeps). Surface plots of dF/F of the ROI with 4 by 4 binned pixels (bottom). **i,** Scheme of ChR2 injection in VMH and ChR2 expressing somas in VMH (left, Scale is 10 µm). **j,** Scheme of the experiment (left), stimulating VMH neuron with 473 nm and 585 nm light during cell-attached recording (right). Illumination with 473 nm was able to activate ChR2, but 585 nm light did not evoke a response. **k,** Scheme of experiment (left), ChR2-expressing VMH neuron during whole-cell patch-clamp recording and optogenetic stimulation with 473 nm and 585 nm light (right). Gray area is enlarged below, 3mW 473 nm light illumination could successfully evoke depolarization, but the same intensity at 585 nm only evoked a small (~1 mV) voltage change. Recordings from top to bottom were stimulated with 3,7,14, 21 mW 585 nm light. The maximum 21 mW light power with 585 nm evoked ~2-3 mV depolarization in the recorded neuron. **l,** Scheme of PAG neuron innervated by ChR2-expressing inhibitory axons from hypothalamus during whole-cell patch clamp recording (left). Right, whole cell patch clamp recordings in voltage-clamp mode. We induced incomplete synaptic release with the first narrower (0.75 ms) 473 nm light stimulation and maximal release with four wider (3 ms) 473 nm stimulations. 585 nm light with 0 mW, 10 mW and 20 mW illuminated the recorded neuron during repetition of the incomplete release OS protocol. We confirmed that synaptic ChR2 illuminated by 20 mW 585 nm light did not activate to result in a maximal transmitter release. **m,** Excitation and emission profile of ChR2 (blue) and JF-585 (orange). **n,** Each 473 nm light pulse during 585 nm illumination of the Voltron sensor induced a narrow “blue spike” artefact. These serve as time stamps of optogenetic stimulation and are reversed in polarity to v-APs, analysis removes them from all Voltron recordings.

Extended Data Figure 2: Axonal mapping, burst detection, concentric analysis, clustering parameters

All Voltron traces were reversed. **a,** Scheme of pAAV-Ef1a-eYFP injection to VMH. Heat maps of VMH axonal density in the PAG along the A-P axis. **b,** 3D reconstruction of VMH axonal density in the PAG, color codes density from blue (low) to red (high). **c,** A-P coordinates of imaging planes with 6911 imaged neurons (Dots in the planes are showing the individual imaged neurons (6911 neurons/ 7 animals). **d,** a Voltron-expressing neuron in the PAG during all-optical imaging and whole-cell patch-clamp recording. Corresponding v-phys (gold) and e-phys (black) sweeps, magenta dots show the detected peaks, green lines under the v-phys recording indicate the detected bursts (left). Box plot shows the difference between the frequency of ISIs where burst was detected (green dots) compared to ISIs where bursts were not detected (gray dots). Dots represent individual ISIs from 6 v-phys sweeps of the shown biocytin labeled neuron (mean±sd t-test, ***p<0.001). Biocytin-filled Voltron-expressing PAG neuron in the ChR2-expressing VMH axonal cloud (bottom). Inserts from top to bottom show ChR2 expression, Voltron expression and biocytin labeling. **f,** 29 parameters derived from the basic parameters used for the hierarchical clustering of v-phys types. **g,** line plot of the number

of clusters as a function of cutoff of the Euclidean distance on the agglomerative clustering dendrogram (blue) and the increment of the number of clusters in the same comparison (green). **h,** dendrogram with the applied Euclidean distance cutoff and the clusters color coded and numbered.

Extended Data Figure 3: Spatial mapping of all-optical connectome

a, Line drawings of the aqueduct (AQ) along the A-P axis of PAG, templated with coronal PAG sections of the Allen reference atlas. **b,** 3D mapping of the all-optical voltage-imaged PAG neurons; FOV with Voltron-expressing neurons illustrate the extraction of X and Y coordinates relative to the top left corner of each FOV (left), A-P coordinate was defined based on the shape of the AQ; reference lines were spaced away by the size of the FOVs (middle), and was used to rail the FOVs upon mapping up to the identified A-P coordinate (left). **c,** 3D mapping of VMH axons in the PAG was used to investigate axonal density and validate the basic anatomy and v-phys correspondence of PAG axonal coverage and postsynaptic response intensity. We filtered our VMH-PAG connectome to extract the two extremes, the "Highest synaptic drive" (>40 Hz firing) and the "No synaptic connection" (no v-PSP or AP). **d,** The "Highest synaptic drive" postsynaptic neurons overlapped with anatomical regions of PAG with high axonal density. **e,** The "No synaptic connection" neurons mapped to PAG regions with sparse axonal coverage. **f,** The observed average minimal distance (AMD) from a neuron to another neuron of the same cluster versus observed average minimal distance (AMD) from a neuron of another cluster comparisons summarized by the number of significant comparisons (* = p-value < 3*10^-5) per cluster. **g,** 3D PAG model of one hemisphere for v-phys cluster 1,5,8 with the density-core mapping of postsynaptic neurons colored by cluster identity (left), coronal bins of PAG (1: -3,25- -3,65 2: -3,65- -3,95; 3:-3,95- -4,25; 4: -4,25- -4,55, 5: -4,55- -4,85, 6: -4,85- -5,15 mm to Bregma) merging the spatial coordinates of cluster 1,5 and 8 (right). **h,** 3D PAG model of one hemisphere for v-phys cluster 6,9 with the density-core mapping of postsynaptic neurons colored by cluster identity (left), coronal bins of PAG (2: -3,65- -3,95; 3:-3,95- -4,25 mm to Bregma) merging the spatial coordinates of cluster 1,5 and 8 (right).

Extended Data Figure 4: Spatial mapping of all-optical connectome

a, In situ hybridization (ISH) images of A-P coordinates of PAG implemented from the open source Allen ISH database with inversed colors for better visibility. Indicated genes from top to bottom: *Gad1, Gad2, Slc32a1, Slc17a6*. PAG subregions are labeled on each picture with "d" for dPAG, "dl" for dlPAG and "l" for lPAG. **b,** Scatter plots of detected genes per number of reads in Smart-Seq2 (top) and Smart-Seq3 (bottom) library preparation protocols. **c,** Bar plot of Voltage-Seq RNA-transcriptome with the expression of *Voltron-ST, Slc32a1, Gad2, Gad1, Slc17a6 and glial markers Olig2, Hopx, Gfap, Agp4, Aldh1l1, Sox10*. Minor ticks are 5 and 10 TPM from left to right for each gene.

Csillag *et al.* - Figure 1.

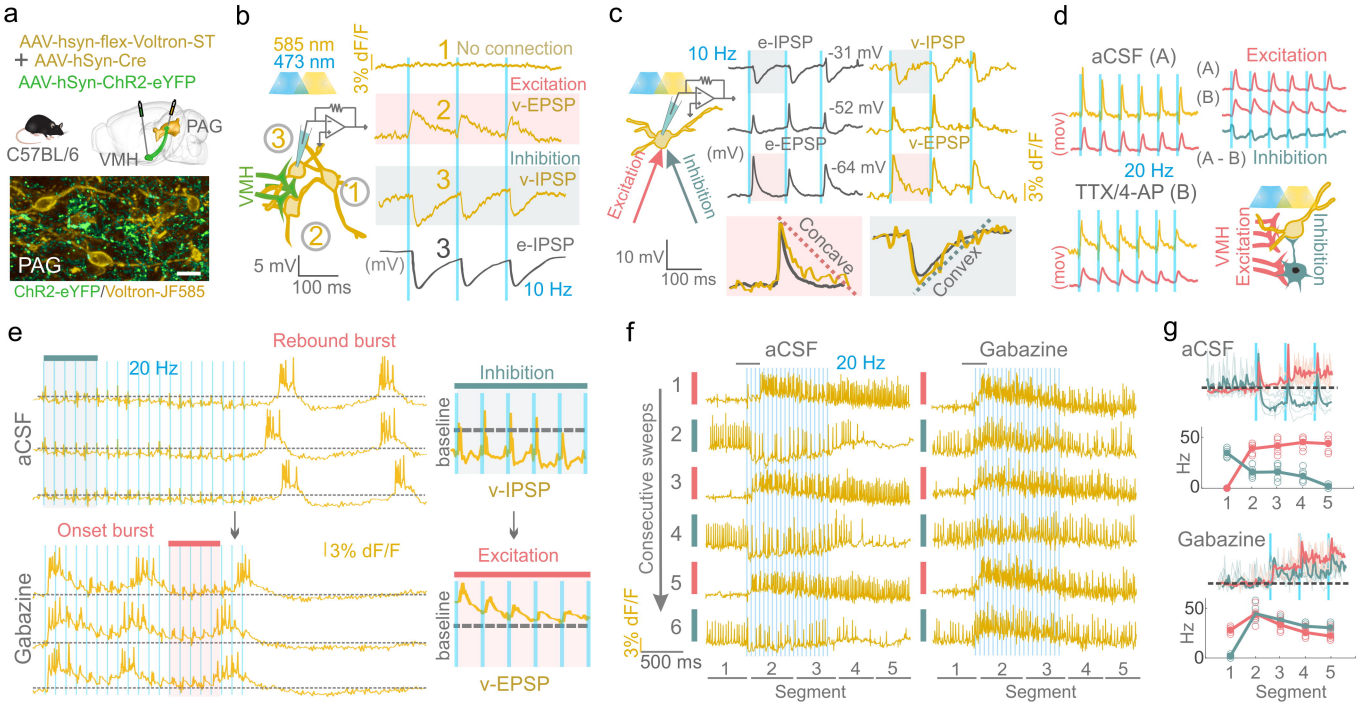

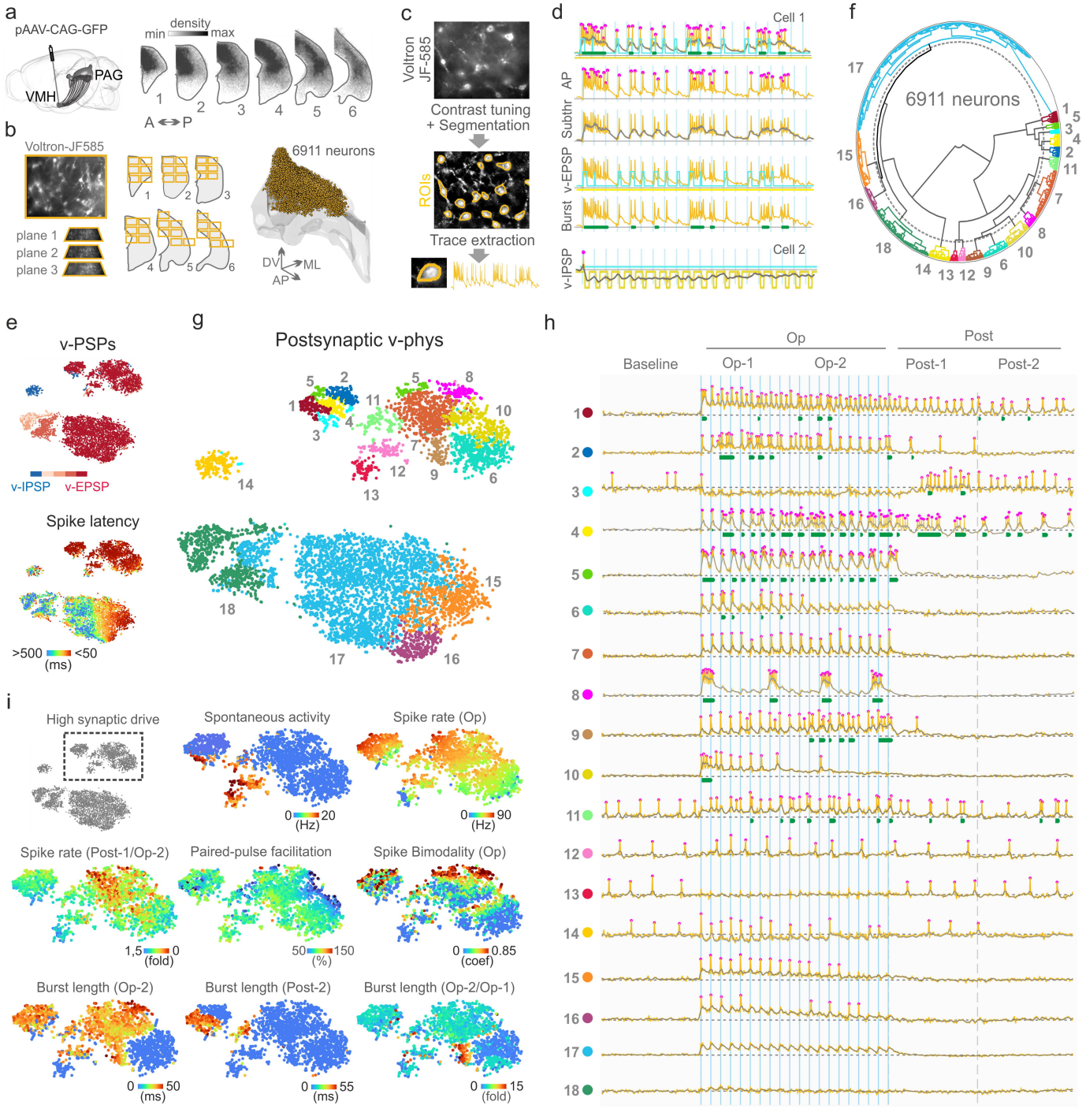
a
pAAV-CAG-GFP
VMH
PAG
density
min
max
1
2
3
4
5
6
A ↔ P
b
Voltron-JF585
plane 1
plane 2
plane 3
6911 neurons
DV
ML
AP
c
Voltron JF-585
Contrast tuning + Segmentation
ROIs
Trace extraction
d
Cell 1
AP
Subthr
v-EPSP
Burst
Cell 2
v-IPSP
f
6911 neurons
e
v-PSPs
v-IPSP
v-EPSP
Spike latency
>500
<50
(ms)
g
Postsynaptic v-phys
h
Baseline
Op
Op-1
Op-2
Post
Post-1
Post-2
i
High synaptic drive
Spontaneous activity
0
20
(Hz)
Spike rate (Op)
0
90
(Hz)
Spike rate (Post-1/Op-2)
1,5
0
(fold)
Paired-pulse facilitation
50
150
(%)
Spike Bimodality (Op)
0
0.85
(coef)
Burst length (Op-2)
0
50
(ms)
Burst length (Post-2)
0
55
(ms)
Burst length (Op-2/Op-1)
0
15
(fold)

Csillag *et al.* - Figure 3.

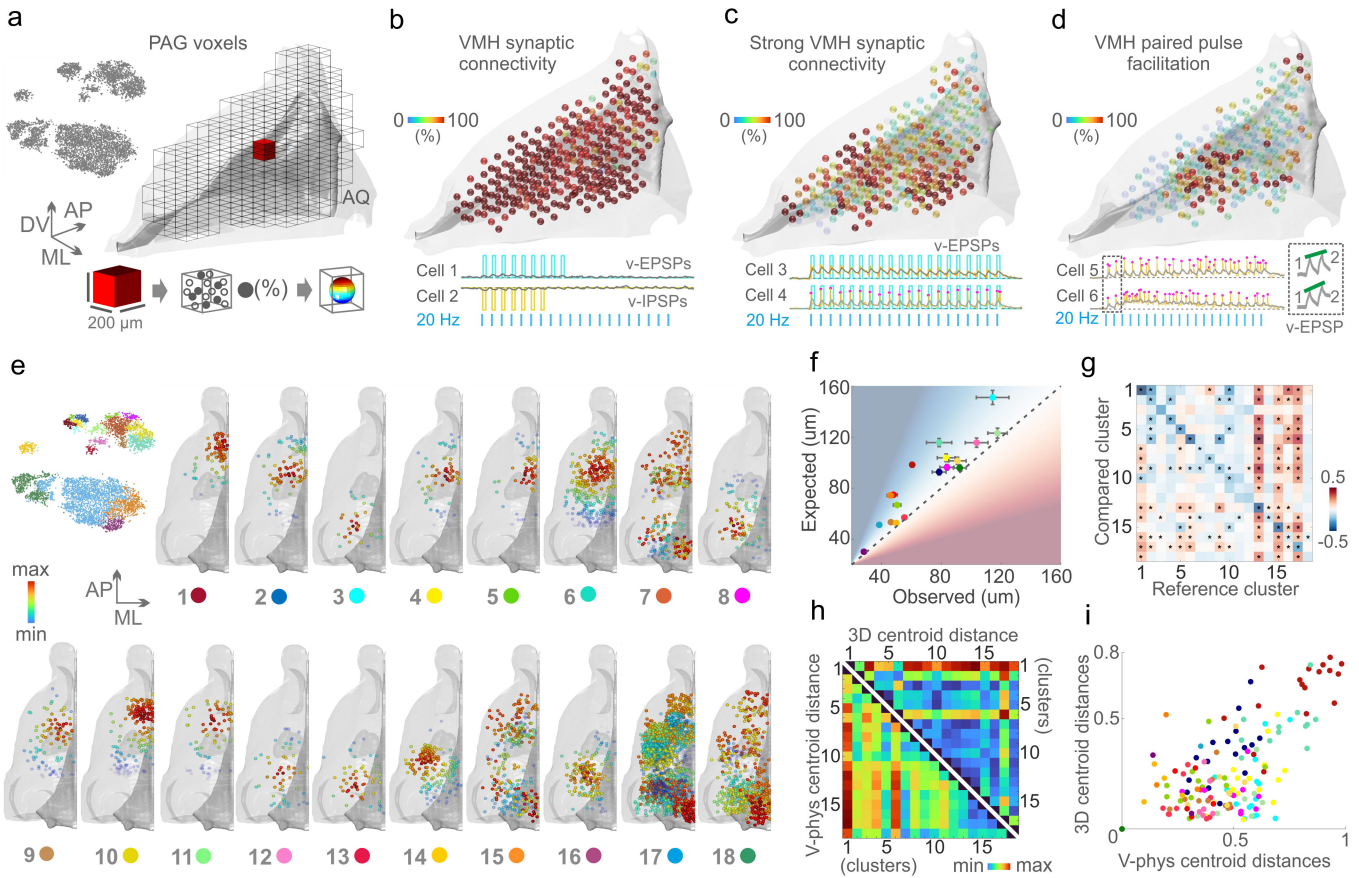

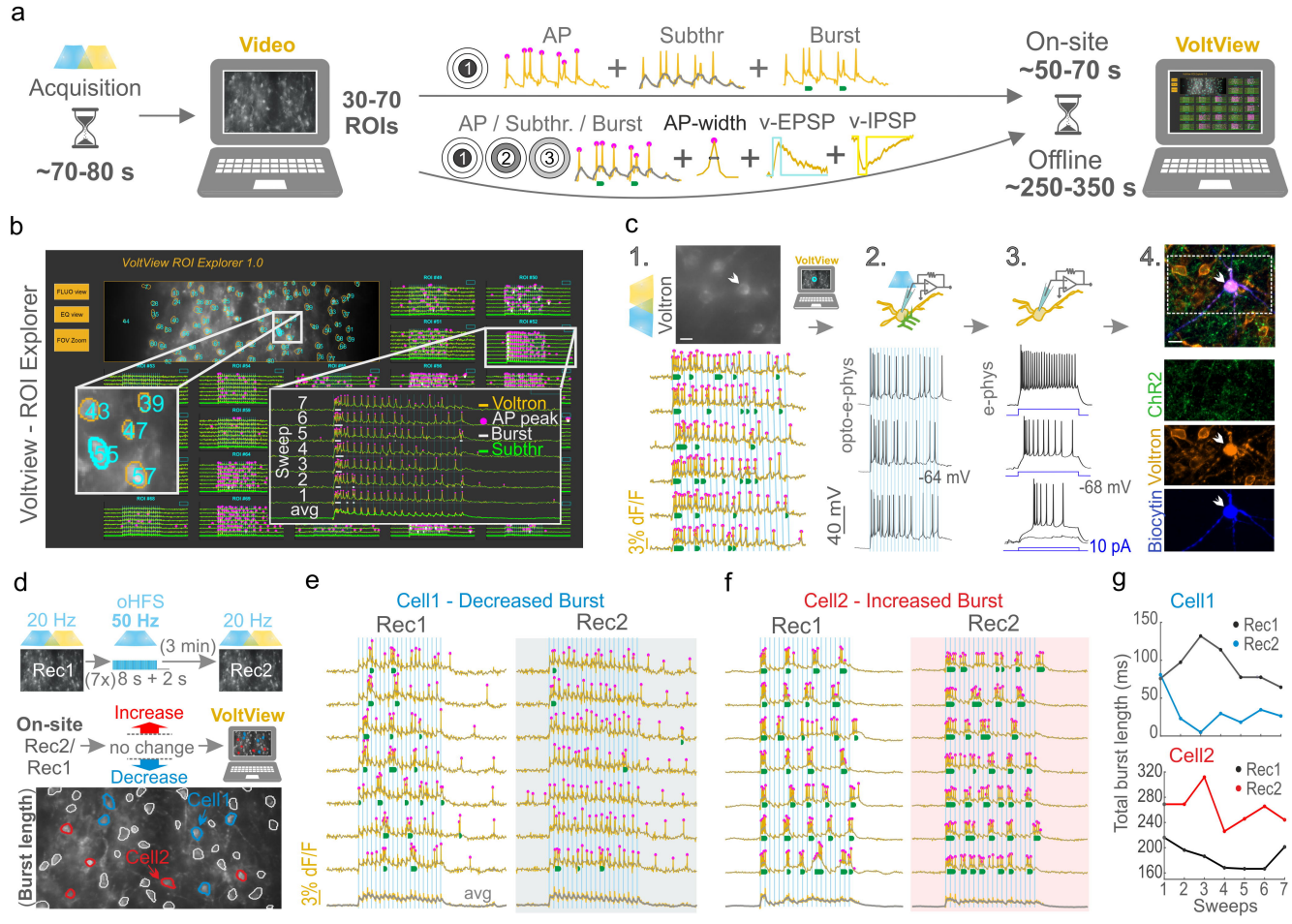
a
Acquisition
~70-80 s
Video
30-70 ROIs
AP
Subthr
Burst
AP / Subthr. / Burst
AP-width
v-EPSP
v-IPSP
On-site
~50-70 s
Offline
~250-350 s
VoltView
b
Voltview - ROI Explorer
VoltView ROI Explorer 1.0
FLUO view
EQ view
FOV Zoom
Sweep
avg
Voltron
AP peak
Burst
Subthr
c
1.
Voltron
VoltView
2.
3.
4.
opto-e-phys
e-phys
-64 mV
-68 mV
40 mV
10 pA
3% dF/F
ChR2
Voltron
Biocytin
d
20 Hz
oHFS
50 Hz
20 Hz
(3 min)
Rec1
(7x)8 s + 2 s
Rec2
On-site
Rec2/ Rec1
Increase
no change
Decrease
VoltView
(Burst length)
Cell1
Cell2
e
Cell1 - Decreased Burst
Rec1
Rec2
3% dF/F
avg
f
Cell2 - Increased Burst
Rec1
Rec2
g
Cell1
Rec1
Rec2
Total burst length (ms)
Cell2
Rec1
Rec2
Sweeps

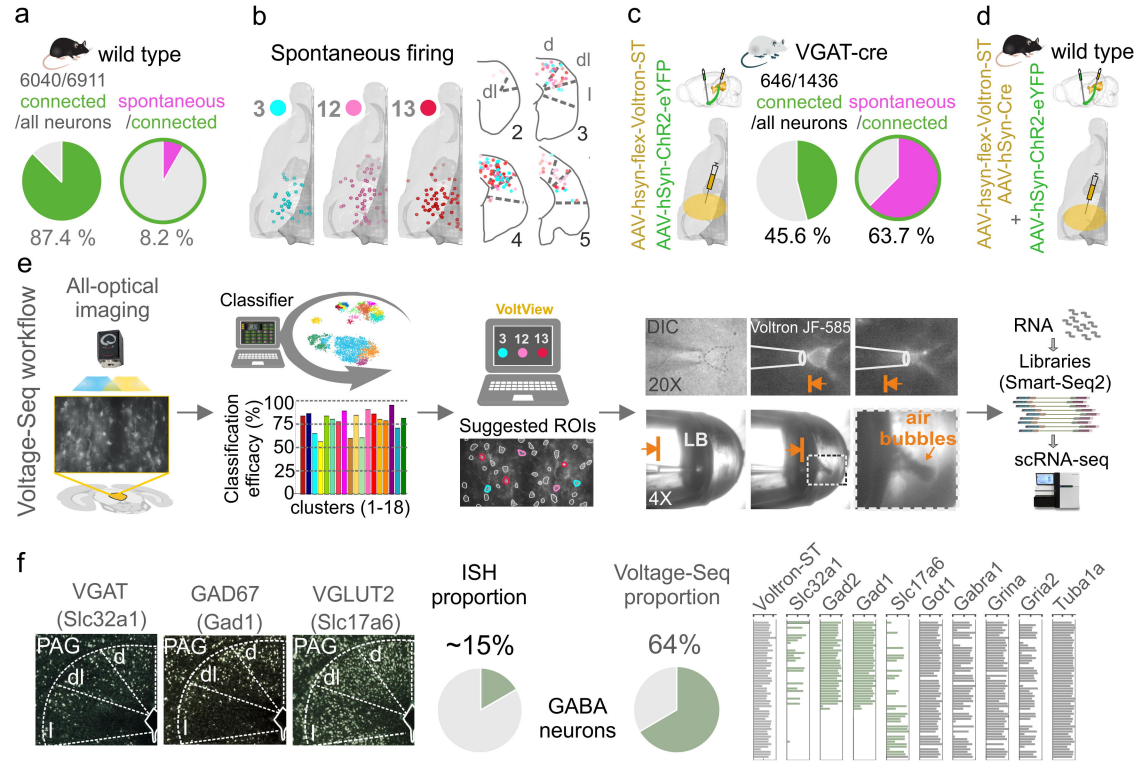
a
wild type
6040/6911
connected /all neurons
spontaneous /connected
87.4 %
8.2 %
b
Spontaneous firing
3
12
13
d
dl
l
2
3
4
5
c
VGAT-cre
646/1436
connected /all neurons
spontaneous /connected
45.6 %
63.7 %
AAV-hsyn-flex-Voltron-ST
AAV-hSyn-ChR2-eYFP
d
wild type
AAV-hsyn-flex-Voltron-ST
AAV-hSyn-Cre
+
AAV-hSyn-ChR2-eYFP
e
Voltage-Seq workflow
All-optical imaging
Classifier
Classification efficacy (%)
100
75
50
25
0
clusters (1-18)
VoltView
3 12 13
Suggested ROIs
DIC
20X
Voltron JF-585
LB
4X
air bubbles
RNA
Libraries (Smart-Seq2)
scRNA-seq
f
VGAT (Slc32a1)
GAD67 (Gad1)
VGLUT2 (Slc17a6)
PAG
d
dl
l
ISH proportion
~15%
GABA neurons
Voltage-Seq proportion
64%
Voltron-ST
Slc32a1
Gad2
Gad1
Slc17a6
Got1
Gabra1
Grina
Gria2
Tuba1a

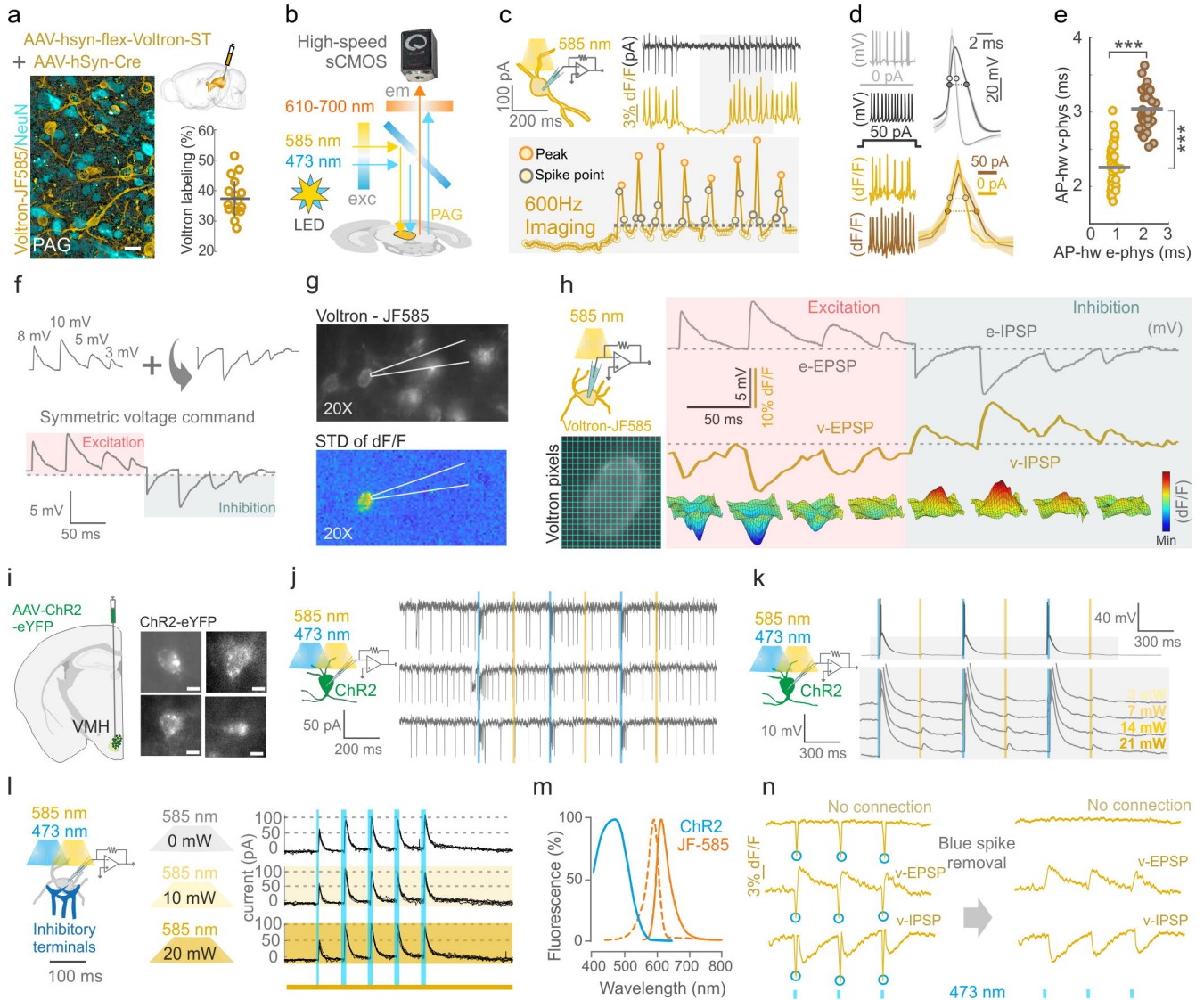
a
AAV-hsyn-flex-Voltron-ST
+ AAV-hSyn-Cre
Voltron-JF585/NeuN
PAG
Voltron labeling (%)
b
High-speed sCMOS
em
610-700 nm
585 nm
473 nm
exc
LED
PAG
c
585 nm
100 pA
200 ms
3% dF/F(pA)
Peak
Spike point
600Hz Imaging
d
(mV)
0 pA
50 pA
2 ms
20 mV
(dF/F)
e
AP-hw v-phys (ms)
AP-hw e-phys (ms)
***
f
10 mV
8 mV
5 mV
3 mV
Symmetric voltage command
Excitation
Inhibition
5 mV
50 ms
g
Voltron - JF585
20X
STD of dF/F
h
585 nm
Voltron-JF585
Voltron pixels
Excitation
Inhibition
e-IPSP
e-EPSP
v-EPSP
v-IPSP
(mV)
5 mV
10% dF/F
50 ms
(dF/F)
Min
i
AAV-ChR2 -eYFP
ChR2-eYFP
VMH
j
585 nm
473 nm
ChR2
50 pA
200 ms
k
585 nm
473 nm
ChR2
40 mV
300 ms
10 mV
3 mW
7 mW
14 mW
21 mW
l
585 nm
473 nm
Inhibitory terminals
100 ms
585 nm
0 mW
585 nm
10 mW
585 nm
20 mW
current (pA)
m
ChR2
JF-585
Fluorescence (%)
Wavelength (nm)
n
No connection
Blue spike removal
3% dF/F
v-EPSP
v-IPSP
473 nm

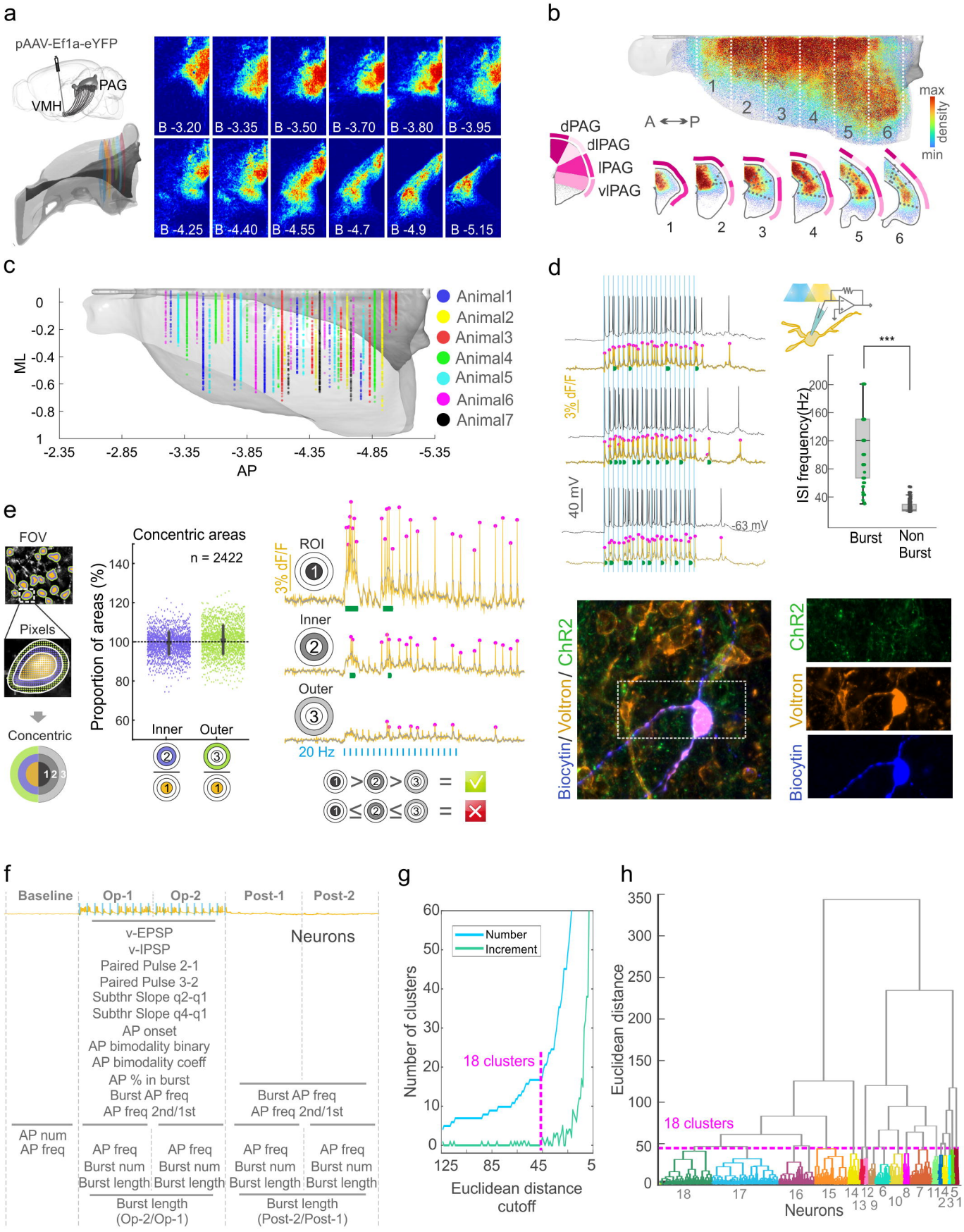
a
pAAV-Ef1a-eYFP
PAG
VMH
B -3.20
B -3.35
B -3.50
B -3.70
B -3.80
B -3.95
B -4.25
B -4.40
B -4.55
B -4.7
B -4.9
B -5.15
b
dPAG
dlPAG
lPAG
vlPAG
A ↔ P
max
density
min
c
ML
AP
Animal1
Animal2
Animal3
Animal4
Animal5
Animal6
Animal7
d
3% dF/F
40 mV
-63 mV
ISI frequency(Hz)
Burst
Non Burst
Biocytin/ Voltron/ ChR2
ChR2
Voltron
Biocytin
e
FOV
Pixels
Concentric
Concentric areas
n = 2422
Proportion of areas (%)
Inner
Outer
ROI
20 Hz
f
Baseline
Op-1
Op-2
Post-1
Post-2
Neurons
v-EPSP
v-IPSP
Paired Pulse 2-1
Paired Pulse 3-2
Subthr Slope q2-q1
Subthr Slope q4-q1
AP onset
AP bimodality binary
AP bimodality coeff
AP % in burst
Burst AP freq
AP freq 2nd/1st
AP num
AP freq
Burst num
Burst length
Burst length (Op-2/Op-1)
Burst length (Post-2/Post-1)
g
Number
Increment
Number of clusters
18 clusters
Euclidean distance cutoff
h
Euclidean distance
18 clusters
Neurons

Csillag *et al.* - Extended Data Figure 3.

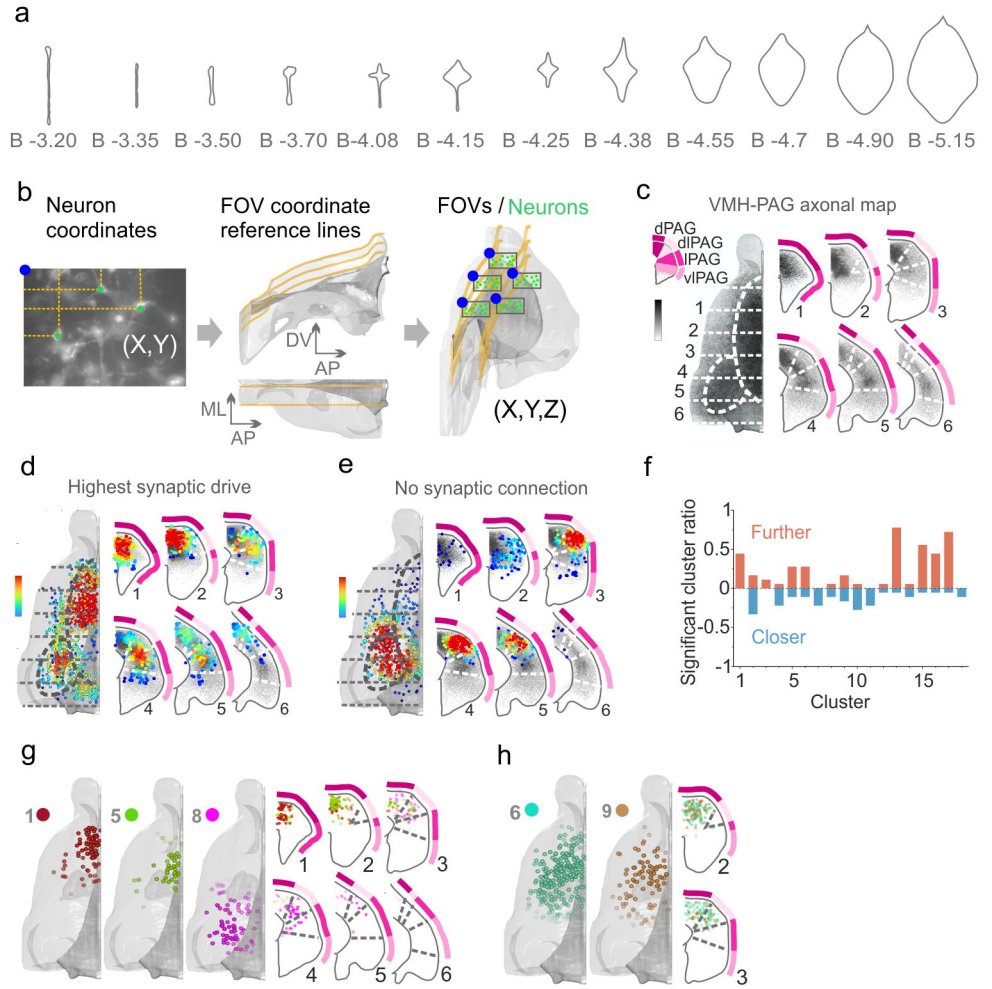

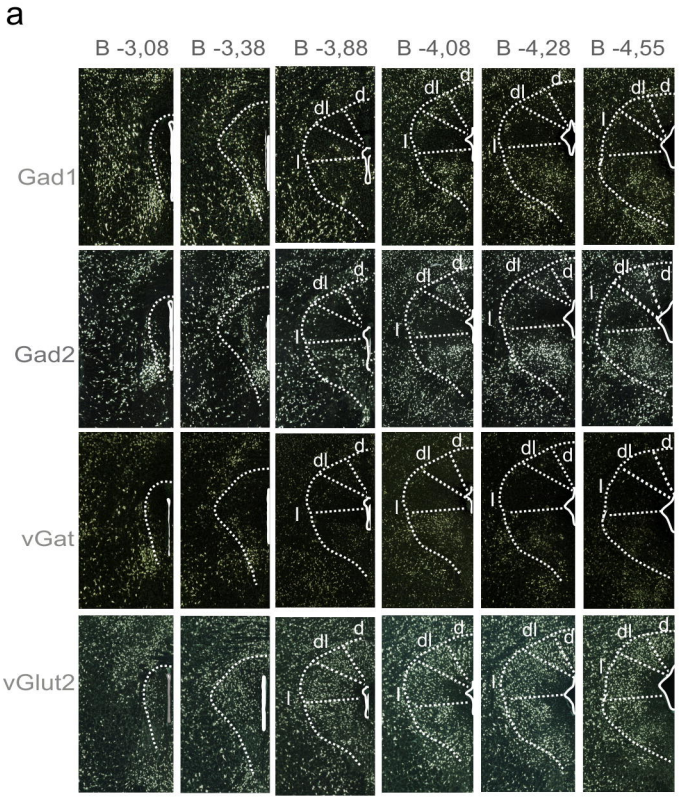
a
B -3,08
B -3,38
B -3,88
B -4,08
B -4,28
B -4,55
Gad1
Gad2
vGat
vGlut2
dl
d
l

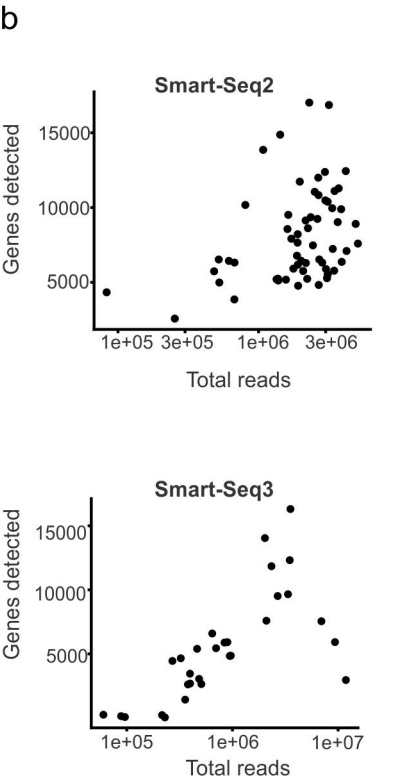
b
Smart-Seq2
Genes detected
15000
10000
5000
1e+05
3e+05
1e+06
3e+06
Total reads
Smart-Seq3
Genes detected
15000
10000
5000
1e+05
1e+06
1e+07
Total reads

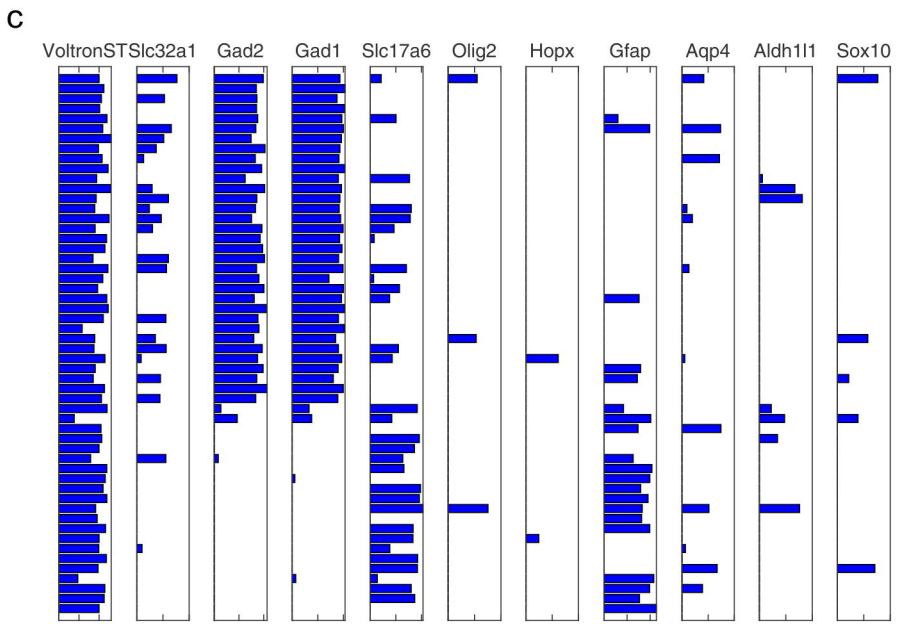
c
VoltronST
Slc32a1
Gad2
Gad1
Slc17a6
Olig2
Hopx
Gfap
Aqp4
Aldh1l1
Sox10